The Impacts of Demand Side Management on Combined Frequency and Angular Stability of the Power System

The Impacts of Demand Side Management on Combined Frequency and Angular Stability of the Power System

Mengxuan Wang, *Student Member, IEEE*, Jovica V. Milanović, *Fellow, IEEE*

***Abstract*—Demand Side Management (DSM) has attracted significant attention over the past decade due to its potential contributions to power systems stability and flexibility improvement. The impact of DSM on system stability is traditionally assessed from one or two stability aspects, which may lead to less than comprehensive understanding and ambiguous deployment decisions that subsequently, deteriorate and even endanger system stability. This paper assesses the impact of transmission level advanced DSM on combined system angular and frequency stability using a newly proposed composite stability index. The versatility of the proposed composite stability index and the critical factors (i.e., penetration level of Renewable Energy Source (RES) and modelling of system demand) influencing the impact of advanced DSM on combined system stability are identified using a range of case studies. Such studies were conducted under different operating conditions based on a modified IEEE 68-bus test system and an equivalent network comprising four interconnected real power systems in a mixed environment of Matlab and DigSilent PowerFactory.**

***Index Terms*-- Composite Index, Demand Side Management, System stability, Probabilistic Analysis.**

I. Introduction

THE operation of modern power systems is evolving rapidly to be more environmentally friendly, more flexible and more economical. In the meantime, operational flexibility and stability of power systems are challenged by the ever-growing integration of temporally and spatially varying generations (e.g., Renewable Energy Sources (RES)-based generations) and demands (e.g., Electric Vehicles (EV)). The traditional way of maintaining system flexibility and stability may become inefficient with the decommissioning of fossil fuel-based synchronous generators. Therefore, additional supports, for instance, Demand Side Management (DSM), which alters electricity consumption patterns of grid customers to produce desired changes of system operational or financial performance, have gained substantial attention during the past decade in order to enhance and improve power system operational flexibility and stability performance [1].

This work was supported by the EU Horizon 2020 Project CROSSBOW, Grant Agreement 773430.

The authors are with the Department of Electrical and Electronic Engineering, The University of Manchester, Manchester M13 9PL, U.K. (email:mengxuan.wang@postgrad.manchester.ac.uk; milanovic@manchester.ac.uk).

The impacts of DSM on different aspects of power system stability have been investigated in many previous research papers [2–7]. A load re-scheduling and emergency load shedding strategy is proposed in [2] to improve system security and the voltage stability margin. An improved DSM program with the consideration of day-ahead weather and load forecast can be found in [3] with its considerable benefits on short-term voltage stability performance. DSM is also commonly adopted for system frequency regulations. In [4], a distributed pinning DSM strategy is integrated into the secondary frequency control to improve the operational performance of power plants. While in [5], DSM is introduced to achieve faster stabilisation of system frequency; the novel algorithm is characterised by its independency from a centralised control and complex communication infrastructure. In terms of system rotor angle stability, different types of loads (constant impedance and Induction Motor (IM) loads) are shifted in [6], which leads to deteriorated small-disturbance stability performance at both peak (high demand) and off-peak (low demand) hours. The contribution of DSM to transient stability is studied in [7] by comparing critical fault clearing time and maximum rotor angle deviation before and after DSM implementation. All the above-mentioned research focusses on one particular aspect of system stability by neglecting the impacts of DSM on all other stability aspects.

By altering electricity consumption patterns and demand compositions, a power system moves to a new operating condition and all system stability aspects get affected simultaneously. Therefore, a comprehensive analysis of the impact of DSM on system stability should cover multiple stability aspects. For instance, a hierarchical power flow control architecture that involves DSM is proposed in [8]; the benefits of DSM are assessed by maximum angle deviation, frequency nadir and a minimum damping ratio for transient stability, frequency stability and small-disturbance stability, respectively. Moreover, the authors of [9] rank load demand (active power) of all demand buses affecting voltage and small-disturbance stability by applying a Morris screening-based sensitivity analysis. It has been found that altering the active power at one certain location can affect system voltage and small-disturbance stability performance to different extents. Similarly, simultaneous analysis of voltage and frequency stability are performed in [10] based on an interconnected hybrid power system in the presence of

Flexible Alternative Current Transmission System (FACTS) devices and DSM. The quantitative analysis of results indicates that the DSM scheme is more effective in affecting frequency stability than voltage stability [10]. Although these studies have considered multiple aspects of system stability simultaneously, different aspects of system stability are assessed separately by corresponding stability indices. Because DSM results in different and even opposite impacts on different aspects of system stability, there is clearly a need to combine and balance the various impacts of DSM on individual stability aspects in order to obtain a more comprehensive understanding of DSM implementations and make more beneficial dispatch decisions.

This paper aims to assess the overall impacts of advanced DSM on combined system stability, which considers system angular and frequency stability simultaneously, in various operating and modelling conditions (e.g., different system renewable penetration levels and different models of load demand) using a proposed composite stability index. The proposed composite stability index is a combination of four well established and widely accepted stability indices for individual stability aspects and it assesses multiple stability aspects simultaneously such that different and even opposite impacts on system stability can be properly balanced or prioritised. In this paper, the term 'advanced DSM' refers to comprehensive and realistic modelling of DSM programs (e.g., taking account of demand composition, modelling and payback effects). The proposed composite stability index and modelling of advanced DSM can be easily applied to other systems and studies beyond the power system stability. To the best of the authors' knowledge, this is the first paper that models practical aspects of DSM application at transmission level and assesses the impact of transmission level DSM not only on single, but also multiple system stability aspects simultaneously using a composite stability index. A Monte Carlo simulation (MCS)-based probabilistic analysis method covering several critical operational uncertainties is adopted in this paper to derive reasonable and reliable operating conditions based on a modified IEEE 68-bus test system with integrated RES generation and on a 4TNE (Transmission Network Equivalent) system representing four interconnected real transmission networks. All simulations are performed in a mixed Matlab/DigSilent PowerFactory environment.

II. System Stability and Composite Stability Index

The proposed composite stability index evaluates combined system stability from three aspects, namely small-disturbance stability, transient stability (also known as large-disturbance stability) and frequency stability simultaneously. Each stability aspect is represented by normalised distances to a corresponding stability limit (i.e., the boundary between stable and unstable) while relying on widely adopted stability index (indices).

A. Stability Indices and Corresponding Limits

1) *Small disturbance stability* is usually assessed by damping (real part of the conjugate eigenvalues) of the most critical electromechanical mode or the damping factor [11]. Both indices can be derived from the critical conjugate eigenvalues, shown as λ in (1), of the linearised system state matrix. Power systems are considered small-disturbance unstable when the critical eigenvalues (λ) moves from the left-hand side (negative σ) to the right-hand side (positive σ) of the complex plane [12]. Consequently, the stability limit for small-disturbance stability can be considered as σ=0. σ is adopted to assess small-disturbance stability performance in the composite stability index.

$$\lambda = \sigma \pm j\omega \tag{1}$$

2) *Transient stability* for individual generators can be evaluated by various stability indices derived from rotor angle excursion following a disturbance, for instance, maximum angle deviation, critical clearing time [13] and settling time. For large power systems, transient stability is usually assessed by the Transient Stability Index (TSI), as shown in (2). Where δ_{max} and δ_{limit} (either 180^o in centre of inertia reference frame [14] or 360^o when rotor angle separation between individual generators is concerned [15]) are the maximum angle deviation and the maximum allowable angle deviation between any two generators during rotor excursion measured in degrees. Power systems are considered transient unstable when the maximum angle deviation (δ_{max}) exceeds the limit (δ_{limit}), in other words, when the TSI is negative. In this study, the TSI has been adopted to evaluate system transient stability and the δ_{limit} is assumed to be 360^o.

$$TSI = \frac{\delta_{limit} - \delta_{max}}{\delta_{limit} + \delta_{max}} \times 100 \tag{2}$$

3) *Frequency Stability* can be evaluated by stability indices derived from frequency excursions. The frequency nadir (zenith) is defined as the lowest (highest) frequency value during the frequency excursions, while the Rate of Change of Frequency (RoCoF) measures the rate of frequency changes within a pre-defined time window. This study focuses on frequency nadir and RoCoF because the disturbances adopted for MCS always result in a frequency drop. In terms of the stability limits, 47 Hz [16] and $\pm$1 Hz/s [17] have been adopted for frequency nadir and RoCoF, respectively. Furthermore, it is assumed that the time window for RoCoF measurement is 100 ms [18], consequently, RoCoF can be derived according to (3), where f_t and f_{t+100} are the frequency values (in Hz) of the start (instant t) and the end (100 ms after instant t) of RoCoF measurement window, respectively. 0.1 is the size of the measurement window in second. Because system frequency stability limits can be defined based on both frequency nadir and RoCoF, frequency stability assessment in this study relies on both indices.

$$RoCoF = \frac{f_{t+100} - f_t}{0.1} \quad (3)$$

All adopted stability indices and corresponding stability limits from individual aspects of system stability can be substituted and adjusted without any loss of generality.

B. Composite Stability Index

As mentioned previously, the proposed composite stability index (i.e., Parallel Circuit Inspired Composite Stability Index (PCICSI)) combines all concerned aspects of system stability based on normalised distances of individual stability indices to corresponding stability limits. The normalisation process is performed according to (4) to (7) for positive mean values of stability indices, where σ, *TSI*, *FN*, *RoCoF* are mean values of individual stability indices obtained from the MCS-based probabilistic analysis at each operating condition. σ'_{Ref}, TSI'_{Ref}, FN'_{Ref} and $|RoCoF'_{Ref}|$ are the reference values for the normalisation, representing the best stability performance (i.e., the largest distance to corresponding stability limits) observed from all simulation results obtained. Stability limits adopted in this study are represented by σ_{Limit}, TSI_{Limit}, FN_{Limit} and $|RoCoF_{Limit}|$ with values of 0, 0, 47 and 1, respectively. In equations (4) to (7), prime (apostrophe) symbol is used to represent stability distance to corresponding limit and the nm subscript indicates normalised distance with respect to the maximum value. Finally, if the mean value of any stability index is negative (stability index violates corresponding limit), the normalised stability distance is assumed to be zero.

$$\sigma'_{nm} = \begin{cases} \dfrac{\sigma_{\text{Limit}} - \sigma}{\sigma'_{Ref}}, & \sigma < 0 \\ 0, & \sigma \geq 0 \end{cases} \quad (4)$$

$$TSI'_{nm} = \begin{cases} \dfrac{TSI - TSI_{\text{Limit}}}{TSI'_{Ref}}, & TSI > 0 \\ 0, & TSI \leq 0 \end{cases} \quad (5)$$

$$FN'_{nm} = \begin{cases} \dfrac{FN - FN_{\text{Limit}}}{FN'_{Ref}}, & FN > 47\ Hz \\ 0\,, & FN \leq 47\ Hz \end{cases} \quad (6)$$

$$RoCoF'_{nm} = \begin{cases} \dfrac{|RoCoF_{\text{Limit}}| - |RoCoF|}{|RoCoF'_{Ref}|}, & |RoCoF| < 1\ Hz/s \\ 0\,, & |RoCoF| \geq 1\ Hz/s \end{cases} \quad (7)$$

In order to derive PCICSI, all normalised stability distances (i.e., σ'_{nm}, TSI'_{nm}, FN'_{nm}, and $RoCoF'_{nm}$) are considered as parallel connected impedance, as shown in Fig. 1, because all aspects of system stability are assessed based on the same operating condition. Similar to the equivalent impedance of parallel connected circuit, PCICSI is calculated based on (8), where 1/4 is introduced to represent that all individual stability indices are considered equally important, assuming violations of particular stability limit are equally important. It is worth noting here that different weightings can be adopted to reflect particular concerns of system operators and vulnerabilities of different power systems more accurately. These weighting factors would be system specific and would need to be developed either by using advanced machine learning methodologies for processing available data about past system performance or be informed by the operator's experience, or most likely a combination of the two. It can be seen from (4) to (8) that the best combined system stability (PCICSI = 1) can be obtained when all individual stability indices show the largest distance to the stability limit, while if any stability index indicates an unstable situation, the combined system stability is unstable (PCICSI = 0). For stable systems, PCICSI varies from 0 to 1, and the larger the PCICSI is, the more stable the system is. Voltage stability assessment is not incorporated in the index at present, as it involves different time scales (typically minutes) and different types of analysis (typically gradual load increase).

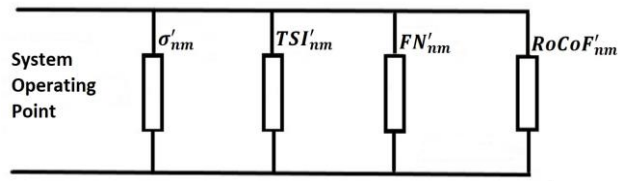

Figure 1: Graphical representation of the structure of PCICSI.

$$\frac{1}{PCICSI} = \frac{1}{4} \times \left(\frac{1}{\sigma'_{nm}} + \frac{1}{TSI'_{nm}} + \frac{1}{FN'_{nm}} + \frac{1}{RoCoF'_{nm}} \right) \quad (8)$$

III. Test Systems under Study

A. Test Systems Overview

The modified IEEE 68-bus test system and the equivalent system adopted in this study are illustrated in Fig. 2 and in Fig. 3, respectively. The IEEE 68-bus test system is modelled at transmission level and consists of 5 interconnected areas, 16 synchronous generators, 35 load buses, 10 Photovoltaic (PV) solar farms modelled as aggregations of Full Converter Connected (FCC) generators and 10 wind farms modelled as a combination of Double Fed Induction Generators (DFIG) and FCC generators. The system load (demand) is divided into large industrial customers and distribution network buses based on their nominal power demands. Out of all load buses, 5 large industrial customer loads and 5 distribution network loads are selected to be flexible demand (i.e., DSM assets). The locations of these DSM assets are marked as red circles and red triangles in Fig. 2 for large industrial customers and distribution networks, respectively. They are selected based on [19] which identified and ranked load buses based on the impact that the variation in their real power demand had on system stability performance.

Synchronous generators in the test system have been divided into four categories, namely gas fired power plant (G1), hydro power plants (G5 and G9), nuclear power plants (G4, G6 and G12) and coal fired power plants (all remaining synchronous generators) with corresponding governors modelled based on real world data [20]. Moreover, a fast-acting static exciter (IEEE STI type) and a Power System Stabiliser (PSS) are installed in G9, while all remaining

synchronous generators are equipped with a slow-acting static exciter (IEEE DC1A type) [20]. Additionally, all generators are operating with a nominal power factor of 0.85 and a spare capacity of 15%. The decommissioning of synchronous generators is determined by the Optimal Power Flow (OPF) results with the objective of minimising the operational cost of synchronous generators. The nominal penetration level of RES generation is 30% of the maximum network load and this value is achieved when all RES-based generators operate at rated output.

The 4TNE system in Fig. 3 represents a reduced order dynamic equivalent model of four interconnected real transmission networks containing 152 buses, 42 synchronous generators (11 hydro and 31 steam/gas generators with corresponding AVRs and governors) and 142 loads. Among all loads, 36 loads (18 large industrial customers and 18 distribution networks) are considered to be flexible, and their locations have been marked as red circles and red triangles in

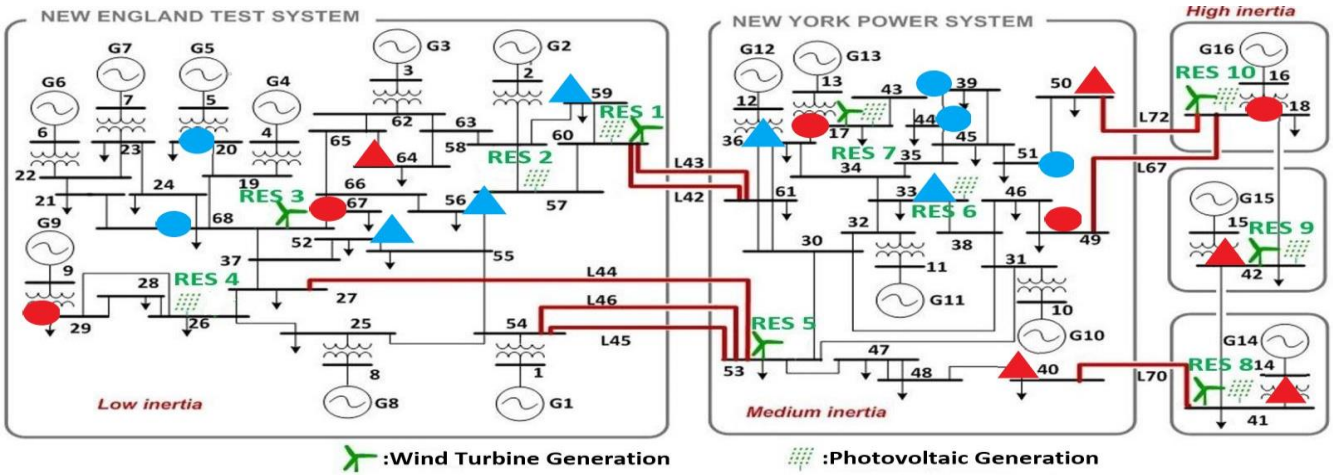

Figure 2: Modified IEEE 68-bus test system with DSM locations emphasised (circles for large industrial customers and triangles for distribution networks).

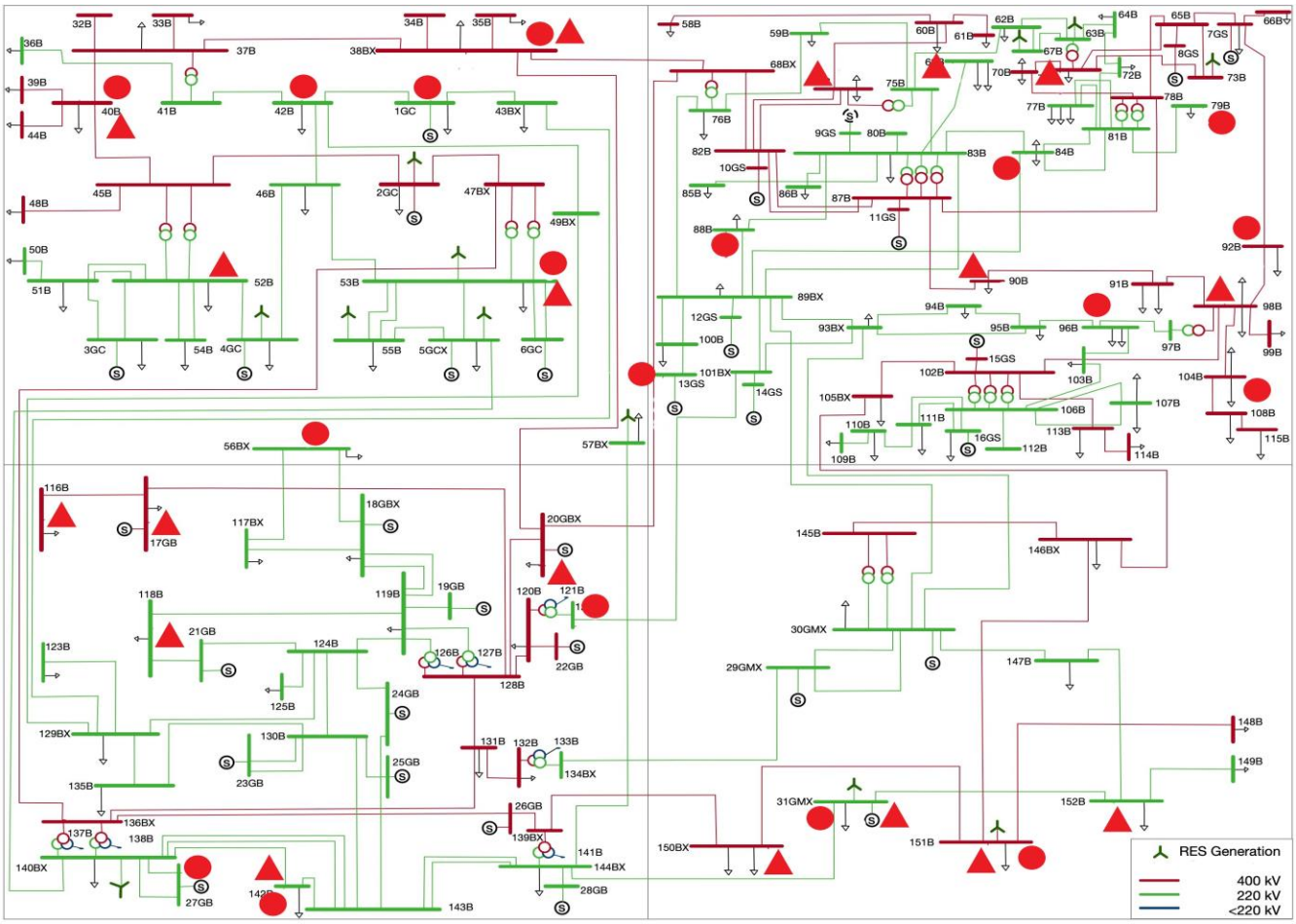

Figure 3: 4TNE equivalent power system with DSM locations emphasised (circles for large industrial customers and triangles for distribution networks).

Fig. 3 for large industrial customers and distribution networks, respectively, Model parameters are either provided by or adopted through consultations with corresponding Transmission System Operators (TSOs). The nominal penetration level of RES generation is 6% of the maximum network load when all RES-based generators operate at rated output.

Disturbances adopted for transient stability and frequency stability assessments are self-clearing three-phase short circuit faults with zero fault impedance and reconnection of all available DSM assets at certain operating points, respectively. Different DSM assets were connected at different operating points depending on the available demand flexibility at the time. Because different disturbances have been applied for transient and frequency stability assessments, stability indices and corresponding stability distances adopted in PCICSI are independent.

B. Modelling of Uncertainties

Several system operational uncertainties have been considered and modelled in an MCS-based probabilistic analysis. First of all, wind speed at each operating point is sampled hourly throughout the day following a Weibull distribution with a shape parameter (α) of 2.2 and a scale parameter (β) of 11.1 [21]. Then, a normal distribution is introduced at each operating point whose mean value is the sampled wind speed and the standard deviation is 0.033. Wind speeds are transferred into turbine power outputs according to the speed-power curve of Vestas-V80, a variable speed wind turbine with a rated power output of 2 MW [22]. Secondly, power outputs of PV panels (rated as 2 MW) are assumed to follow a Beta distribution with shape parameters a = 13.7 and b = 1.3 [23] at each operating point.

In addition to the generation uncertainties, system load demands at each operating point are modelled following a normal distribution with a standard deviation of 0.033 [24]. The mean value of such normal distribution is adopted from normalised daily loading curves shown as the blue solid line and the black dotted line in Fig. 4 for IEEE 68-bus test system and 4TNE system, respectively [25-27]. Normal distributions utilised for load demands generate scaling factors, which are multiplied by nominal active and reactive powers for all load demands. Finally, and importantly, faulted transmission lines and fault locations along the line are selected randomly for each simulation in transient stability assessment, fault duration is determined following a normal distribution with a mean value of 5 cycles (100 ms for 50 Hz power systems) and a standard deviation of 0.67 cycle [28].

C. Modelling of Advanced Demand Side Management

The aim of this study was to illustrate the potential, realistic effect of advanced DSM on various aspects of system stability. Hence, every effort was made to model both, the capacity and flexibility of advanced DSM as realistically as possible. To that effect, in total, 12 flexible processes (6 from large industrial customers and 6 from distribution networks) have been considered to model flexible demand in the IEEE 68-bus test system. Their DSM capacity, defined as the proportion of flexible demand at a corresponding location, is calculated based on both the annually utilisation rate of the process (in hours) and flexibility (in %) following (9) [29].

$$D = \frac{\sum_1^n \left(\frac{U_n}{8760} \times F_n\right)}{\sum n} \times 100\% \qquad (9)$$

Where D is the DSM capacity (in %) for either larger industrial customers or distribution networks, n is the number of DSM processes adopted, U_n and F_n are the utilisation rate (in hour) and flexibility (in %) of process n, respectively. All DSM processes with corresponding utilisation rate and flexibility are summarised in Table I. The final DSM capacities derived according to (9) for large industrial customers and distribution networks are 55% and 20%, respectively. The amounts of flexible demand (in MW) for each DSM process are calculated based on their contributions to the overall DSM capacity and they are also shown in Table I. It can be seen from Table I that the total capacity of flexible demand is 3126 MW, which is 18% of the network peak demand. In this paper, the term 'flexible demand' refers to the controllable part of the demand only. The actual demand of the process in some cases includes the uncontrollable part of the demand as well. For example, in the first row of Table I, the flexible demand size of the listed process is 78.62 MW and the flexibility of that process is F_n=25%, which means the process is partially flexible. The process listed in row six has a flexible part of 231.45 MW with F_n=100%. Hence, the process is fully flexible.

The DSM programs adopted in this study are load shedding and load shifting. To be more specific, load demand is curtailed without any payback for the load shedding program while in the case of load shifting, load demand is curtailed with demand payback within a certain time interval. Programs of each DSM process and corresponding demand payback profiles are listed in Table I [30], where maximum DSM duration indicates the maximum allowable duration for load curtailment (reconnection); the maximum shiftable time represents the maximum allowable duration between load curtailment and demand payback. The normalised daily loading curve after advanced DSM is shown as the red dashed line in Fig. 4. It can be seen that system demand has been manipulated at 23 out of 24 hours throughout the day. The peak loading can be reduced from 1 p.u. to 0.93 p.u., while the

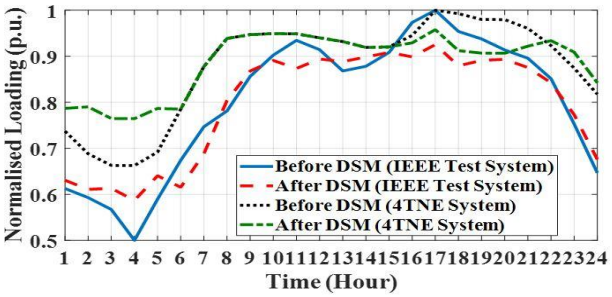

Figure 4: Normalised system daily loading curves before/after DSM [25-27].

minimum loading can be increased from 0.5 p.u. to 0.59 p.u. by the advanced DSM.

In the case of the 4TNE system, DSM profiles, including but not limited to, DSM capacity, DSM programs and locations, are provided by corresponding TSOs based on estimations of availability and flexibility of near future system demands. However, these DSM profiles constrain the development of the DSM implementation plan in the 4TNE system as more requirements need to be met. The total capacity of the flexible demands is 1654 MW, which is 14% of the 4TNE network peak demand and all flexible DSM assets are assumed to be fully controllable. Implementations of advanced DSM (i.e., load shedding and load shifting with the consideration of demand payback) based on the 4TNE system are determined according to [31-33] and the normalised daily loading curve after advanced DSM is shown as the green dash-dot line in Fig. 4. In this case, the system demand has been manipulated at only 14 out of 24 hours. The peak loading can be reduced from 1 p.u. to 0.96 p.u., while the minimum loading can be increased from 0.66 p.u. to 0.76 p.u. by the advanced DSM. The modelling parameters of advanced DSM (e.g., flexible demand size and maximum shiftable time) deployed in the 4TNE system are summarised in Table II.

It is worth noting here that this paper focuses on the impact of transmission level DSM programs. The DSM assets are therefore modelled either as the aggregate loads seen at grid supply point (i.e., including combinations of various flexible DSM processes of customers connected to distribution networks) or large industrial customers connected to transmission networks directly, as shown in Tables I and II. The effect of different individual customer technologies has not been considered as their individual influence would have been difficult to see at transmission level and some forms of aggregation would be required anyway.

D. Modelling of Load Demand

According to the international survey performed in [34], constant power load is one of the most commonly used load models for system dynamic studies worldwide; on the other hand, the composite load model (a parallel connection of static ZIP load model and IM model) provides a more accurate and reliable modelling of load composition. Therefore, constant power load and composite load (an aggregation of a number of IMs connected in parallel with a static ZIP load model) have been used in this study [34].

When all load demands are modelled as a constant power load, DSM deployment does not change load compositions. In terms of a composite load model, the flexible DSM processes are modelled as either a constant impedance load or an IM (as shown in Table I) and consequently, DSM deployment and demand payback change load compositions.

TABLE I: DSM PROCESSES WITH CORRESPONDING MODELLING PARAMETERS FOR THE IEEE 68-BUS TEST SYSTEM [29-30]

Flexible DSM Processes-Large Industrial Customers								
DSM Process	**DSM Program**	**Flexible Demand Size (MW)**	**Utilisation U_n (h)**	**Flexibility F_n (%)**	**Maximum DSM Duration (h)**	**Maximum Shiftable Time (h)**	**Maximum Deployment number per day**	**Modelling of DSM Assets**
Electrolytic Primary Aluminium	Load Shedding	78.62	7065	25	4	N/A	1	Constant Impedance
Chloralkali Process (Amalgam)	Load Shedding	229.63	7370	70	4	N/A	1	Constant Impedance
Chloralkali Process (Membrane)	Load Shedding	196.82	7370	60	4	N/A	1	Constant Impedance
Electric Arc Furnace	Load Shedding	292.43	6570	100	4	N/A	1	Constant Impedance
Wood Pulp Production	Load Shifting	249.26	5600	100	3	24	1	Constant Impedance
Cement Mill	Load Shifting	231.45	5200	100	3	24	1	Induction Motor
Flexible DSM Processes-Distribution Networks								
DSM Process	**DSM Program**	**Flexible Demand Size (MW)**	**Utilisation U_n (h)**	**Flexibility F_n (%)**	**Maximum DSM Duration (h)**	**Maximum Shiftable Time (h)**	**Maximum Deployment number per day**	**Modelling of DSM Assets**
Night Storage Heater	Load Shifting	231.34	1200	100	4	4	3	Constant Impedance
Heat Pump	Load Shifting	347.01	1800	100	2	2	3	Constant Impedance
Warm Water Heating	Load Shifting	74.7	1550	25	4	4	3	Constant Impedance
Air Supply	Load Shifting	424.12	4400	50	1	2	3	Induction Motor
Cold Storages	Load Shifting	696.69	5090	71	2	2	3	Induction Motor
Air Conditioning	Load Shifting	73.74	510	75	1	2	3	Induction Motor

TABLE II: DSM PROCESSES WITH CORRESPONDING MODELLING PARAMETERS FOR THE 4TNE SYSTEM [31-33]

Flexible DSM Processes					
DSM Process	**DSM Program**	**Flexible Demand Size (MW)**	**Maximum DSM Duration (h)**	**Maximum Shiftable Time (h)**	**Maximum Deployment number per day**
Curtailable Industrial	Load Shedding	107.35	4	N/A	1
Shiftable Industrial	Load Shifting	76	3	24	1
Residential Wet Appliances	Load Shifting	94.6	6	24	1
Space and Water Heating	Load Shifting	387.88	12	12	1
Cold Appliances	Load Shifting	189.22	1	2	1
Vitalisation	Load Shifting	160.83	1	2	1
Commercial Refrigeration	Load Shifting	113.52	2	2	1
Hydro Pump Plant	Load Shifting	524	N/A	N/A	1

IV. METHODOLOGY AND CASE STUDIES

A. Methodology

The methodology used in this study is an MCS-based probabilistic stability analysis, which estimates the possible output results by random sampling of input variables following corresponding probability distributions and performing deterministic simulation for each input sample [35].

MCS-based probabilistic analysis is performed hourly throughout the day covering 24 different operating conditions with the consideration of various operational uncertainties. For each operating condition, the size of input variable samples (i.e., the number of deterministic simulations performed for each operating condition) is determined according to the MCS stopping rule as shown in (10) [35], where Φ^{-1}, $\sigma^2(X)$ and $\bar{X}$ representing an inverse Gaussian conditional probability distribution, variance and mean values of the input sample X with a size of N. In this study, a confidence level of 99% (i.e., sample mean error E <0.01) is adopted, resulting in at least 500 simulations for each operating condition.

$$E = \left[\left\{\Phi^{-1}\left(1 - {}^{\delta}/_{2}\right) \times \sqrt{{}^{\sigma^2(X)}/_{N}}/\bar{X}\right\}\right] \qquad (10)$$

The whole MCS-based probabilistic analysis methodology can be illustrated in Fig. 5 (step numbers at the bottom right corner) and summarised in the following steps:

Step 1: Operational uncertainties (500 sets for 500 simulations at each operating condition) are generated using corresponding probability distributions in Matlab.

Step 2: OPF is performed considering generated operational uncertainties (Step 1) in the environment of Matpower [36] for the current operating point and results are exported to DigSilent/PowerFactory for dynamic studies.

Step 3: Modal analysis for small-disturbance stability assessment and Root Mean Squared (RMS) simulations for transient and frequency stability assessment are performed in DigSilent/PowerFactory. RMS simulations last for 15 seconds. System responses are exported to Matlab for further analyses.

Step 4: Stability indices are calculated in Matlab.

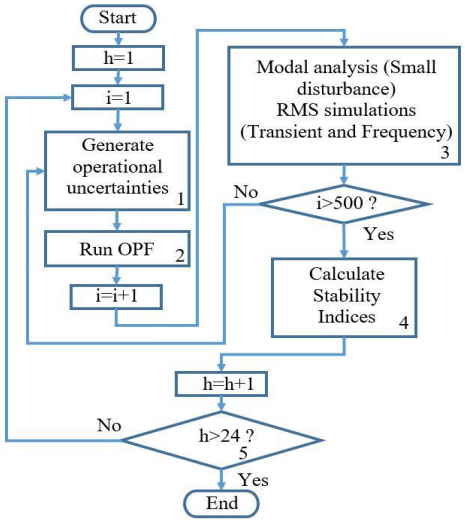

Figure 5: Flow chart of MCS-based probabilistic analysis methodology.

Step 5: Repeat Steps 1 to 4 until all (24) operating points have been covered.

Step 6: Repeat Steps 1 to 5 with advanced DSM deployed and compare calculate composite indices before and after DSM deployments.

B. Case Studies

With the purpose of investigating the impacts of advanced DSM on combined system stability under different operating and modelling conditions, seven case studies have been developed as summarised in Table III where DSM baselines are the proportion of capacity of flexible demands with respect to system peak demand. Cases 1 to 3 are developed to study the performance of advanced DSM under different RES penetration baselines. All RES penetration levels (R) are calculated according to (11) and equal to baselines (as shown in Table III) when all RES generators work at rated power. In (11), P_{RES} and P_{ALL} represent the power generated by RES and all generators, respectively. Due to the uncertain wind speed and solar irradiation, the real RES penetration levels are lower than the baselines and they vary from 3% to 18.6% and from 14.3% to 39% for 30% and 60% RES baseline penetration levels, respectively. Case 4 is developed to study how DSM locations affect their impact on combined system stability. New locations for DSM assets are marked by blue circles and

TABLE III: CASE STUDIES

Case Studies	RES Baseline	DSM Baseline	Load Model	Test System	Note
Case 1	0%	18%	Cnst_Pwr	IEEE	N/A
Case 2	30%	18%	Cnst_Pwr	IEEE	N/A
Case 3	60%	18%	Cnst_Pwr	IEEE	N/A
Case 4	60%	5%	Cnst_Pwr	IEEE	Changed DSM Locations
Case 5	60%	21.6%	Cnst_Pwr	IEEE	1.2 × DSM Capacity
Case 6	60%	18%	Composite	IEEE	N/A
Case 7	6%	14%	Cnst_Pwr	4TNE	N/A

Cnst_Pwr: Constant Power

blue triangles in Fig. 1 for large industrial customers and distribution networks, respectively. Cases 5 and 6 aim to study the impacts of increased (by 20%) DSM capacity and different modelling of load demand, respectively. The impacts of advanced DSM in real power systems are investigated in Case 7. The RES penetration levels in Case 7 vary from 2.3% to 5.8%.

$$R = \frac{P_{RES}}{P_{ALL}} \times 100\% \tag{11}$$

V. RESULTS AND ANALYSIS

A. Illustration of Combined System Stability using Composite Stability Index

As MCS-based probabilistic analyses are performed discretely (i.e., hourly) throughout the day, combined system stability performance is assessed by PCICSI at each hour. Due to the lack of operational information of test systems at shorter time intervals (to an extent) and high computational cost (mostly) associated with performing probabilistic dynamic simulations, the stability assessment is performed and analysed based on discrete hours. The hourly variations of composite stability index in Figs. 6 and 7, illustrating the results of the studies, are presented by a continuous curve (instead of bar charts for example) to improve the clarity of the presentation. In doing this, an assumption has been made that combined system stability performance changes linearly from one operating point to the next. The accuracy of illustration of the results can be easily improved, at a high computational cost though, by performing dynamic simulations at reduced timescales (e.g., every 15 minutes or every 5 minutes) with more detailed and accurate modelling of operational uncertainties (e.g., wind speed). Even though the accuracy of the illustration and calculation of the effect of DSM would improve, the trend and the indication of the size of the effect can still be captured by hourly assessment and adopted continuous line representation.

Daily combined system stability performance for different case studies is illustrated in different subplots of Fig. 6 for the modified IEEE 68-bus test system, while the combined system stability performance for the 4TNE system is illustrated in Fig. 7. It can be seen from Fig. 6 that the combined system stability is mainly affected by the RES baseline (subplots (a) to (c)), locations of DSM assets (subplots (c) and (d)) and load models (subplots (c) and (f)), Variations of DSM capacity (subplots (c) and (e)) have limited impact on combined system stability.

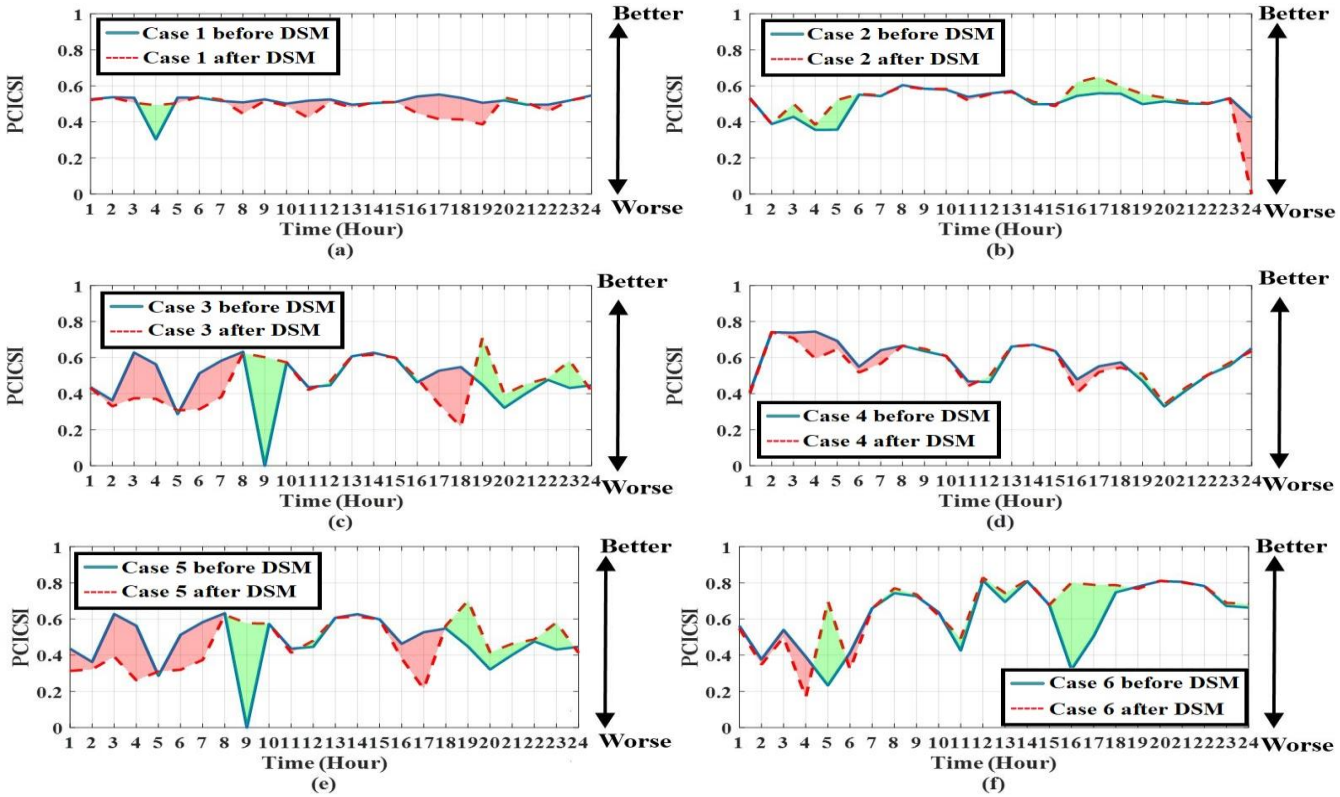

Figure 6: Combined system stability performance illustrated by PCICSI curves for Case 1 (a), Case 2 (b), Case 3 (c), Case 4 (d), Case 5 (e) and Case 6 (f).

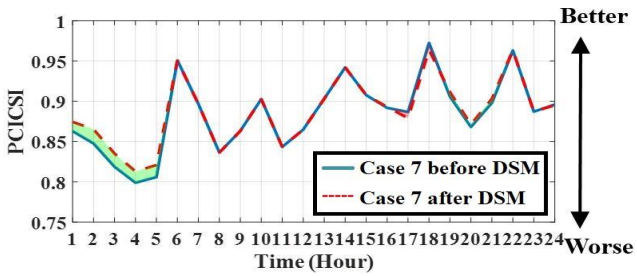

Figure 7: Combined system stability performance illustrated by PCICSI for Case 7.

Additionally, it can be seen from Fig. 7 that the combined system stability of the 4TNE network is not affected very much by DSM as the combined system stability varies in a much smaller range throughout the day. The smaller influence of DSM on system stability performance of this network can be explained by the relatively small size of flexible assets (around 14% of the peak network demand) compared to that of the modified IEEE 68-bus network, where flexible assets equalled 18% of the peak network demand and much smaller penetration of RES generation (6% compared to 30% and 60% in IEEE 68-bus network), whose dynamics and consequential reduction of system inertia affect overall system dynamic response. Furthermore, by considering all stability distances equally important in PCICSI, as shown in (8), frequency stability dominates the performance of PCICSI as two individual stability indices are derived from frequency stability assessment. In the IEEE 68-bus test system, the size of disturbances adopted for frequency stability assessment was 9.5% (maximum 16%) of the total demand at corresponding operating point, leading to FN and RoCoF with minimum values of 46.9 Hz and -0.90 Hz/s, respectively. In the case of the 4TNE system, the corresponding disturbances were smaller, i.e., on average 6% (maximum 9%) of the total demand at the corresponding operating point. The minimum FN and RoCoF values were 49.53 Hz and -0.27 Hz/s, respectively. The reduced size of disturbances reduces the impact of DSM on frequency stability and consequently the impact on combined system stability evaluated by PCICSI.

B. Validation of Proposed Composite Stability Index

In order to validate the proposed composite stability index, daily variations of all individual stability indices considered in PCICSI are illustrated in Fig. 8 for Case 3. In Fig. 8, improved stability performance following the implementation of advanced DSM is marked by a green background and reduced stability performance by a red background.

It can be seen from Fig. 8 that the same DSM action can lead to very different and even opposite impacts on different stability aspects. More specifically, demand paybacks in early morning have limited impact on FN (subplot (c)), but significant impact on RoCoF (subplot (d)). Furthermore, system small disturbance stability (subplot (a)) has been improved at Hours 6 and 7, when all other stability aspects have been weakened. The fact that individual stability aspects are affected very differently by the advanced DSM may affect the decision taken by system operators regarding the effectiveness of DSM deployment at particular time.

Focusing on the subplot (c) of Fig. 6, it can be seen that the combined system stability is mainly reduced by the advanced DSM in early morning as most of the individual stability performance indices are reduced due to the demand paybacks (Fig. 8). Similarly, load curtailment around peak hours (i.e., Hour 17) also deteriorates combined system stability primarily due to reduced system angular stability (subplots (a) and (b) of Fig. 8). On the other hand, because most individual stability aspects can be improved by the advanced DSM around Hour 9 and evening, the combined system stability (subplot (c) of Fig. 6) also exhibits better performance around these time periods.

By comparing Figs. 6 and 8, it can be seen that the proposed composite stability index (i.e., PCICSI) can balance different and opposite impacts of advanced DSM on individual stability aspects efficiently. This can help system operators to have a better understanding of the impacts of advanced DSM on system stability and make DSM investment and implementation decisions accordingly.

C. The Impact of Advanced DSM on Combined System Stability

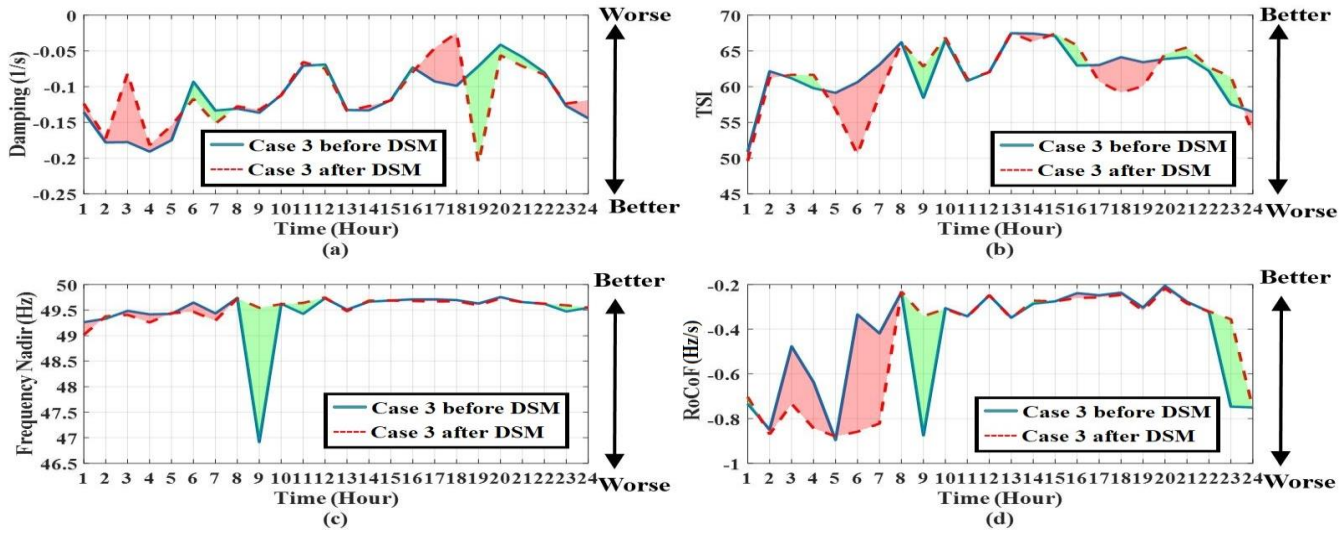

Figure 8: Daily variations of damping (a), TSI (b), FN (c) and RoCoF (d) for Case 3.

By representing daily combined system stability performances as daily PCICSI curves before/after DSM deployment, the impact of DSM on combined system stability can be illustrated by the areas between PCICSI curves before/after DSM deployment. When the PCICSI curve after DSM is higher than (above) the curve before DSM, combined system stability is improved by the DSM deployment and such areas are marked by green backgrounds in Figs. 6 and 7. On the other hand, if the PCICSI curve after DSM is lower than (below) the curve before DSM, DSM is considered to have a deteriorating effect on combined system stability and such areas are marked by red backgrounds in Figs. 6 and 7.

Focusing on the subplot (a) of Fig. 6, it can be seen that advanced DSM can only lead to improved stability performance around off-peak hour (Hour 4) in Case 1 for the test system without RES-based generation. When the test system is operated with 30% RES baseline (subplot (b) of Fig. 6), advanced DSM usually improves the combined system stability performance. Such improvements are more significant around both off-peak and peak hours. In Case 3 (subplot (c) of Fig. 6), DSM deployment can either improve or deteriorate combined system stability performance. In addition to manipulating the magnitude of combined system stability performance, DSM deployment can also lead to system instability (Hour 24 in subplot (b)) and stabilise an unstable system (Hour 9 in subplot (c)).

When advanced DSM is deployed from different locations (subplot (d)), combined system stability performance is affected by a reduced amount (in MW) of DSM deployment, changed locations and reduced sizes of disturbance for frequency stability assessment. Consequently, combined system stability in Case 4 (subplot (d)) is usually better than Case 3 (subplot (c)), especially during off-peak hours (Hours 1 to 8). Regarding the impact of advanced DSM on PCICSI, it can be seen from subplots (c) and (d) of Fig, 6 that different locations of DSM assets mainly result in quantitative changes of PCICSI. More specifically, combined system stability is weakened around off-peak hours (Hours 1 to 8) and early evening (Hours 16 to 18) and improved during daytime (Hours 8 to 15) and late evening (Hours 19 to 24) regardless of DSM locations. It should be noted here that optimising the DSM deployment locations is beyond the scope of this paper.

Similar to Case 4, increased DSM capacity (Case 5 illustrated in the subplot (e) of Fig. 6) also leads to only quantitative changes of DSM impact. However, according to the subplots (c) and (f) of Fig. 6, different load models result in the opposite impact of advanced DSM on combined system stability performance. To be more specific, combined system stability is weakened by the advanced DSM around off-peak hours in the case of constant power load (subplot (c)), while it is improved by the DSM deployment when load demands are modelled as a composite model (subplot (f)) from Hours 4 to 6. Moreover, combined system stability is weakened and improved by advanced DSM around peak hours in Case 3 and Case 6, respectively.

Regarding the 4TNE network (Fig. 7), DSM deployment has a minor impact on combined system stability performance due to the limited DSM implementation (14 out of 24 hours throughout the day) and size of disturbance as discussed in the previous section.

In summary, the impact of advanced DSM on combined system stability can be affected by system RES penetration levels, locations of DSM integration, DSM capacity and modelling of load demand. Among all of the above-mentioned factors, system RES penetration level and modelling of load demand can result in the opposite impact of the same DSM deployment on combined system stability performance. Changes in locations of DSM deployment and DSM capacity, on the other hand, predominantly lead to quantitative difference in the impact but the effect of it (improvement or deterioration of stability) does not change.

D. Quantification of Impact of Advanced DSM on Combined System Stability

Because the beneficial and detrimental impacts of advanced DSM have been represented by the green and red areas illustrated in Figs. 6 and 7, the overall impacts of advanced DSM on combined system stability performance throughout the day can be quantified as the difference between the sum of green areas and the sum of red areas. A negative result indicates a detrimental overall impact of advanced DSM on combined system stability while a positive result represents an overall beneficial impact. The quantified overall impact of advanced DSM on combined system stability is summarised in Table IV. As discussed earlier, the accuracy of this assessment can be improved by using smaller time steps (e.g., every 15 minutes) in assessing the composite stability index.

It can be seen from Table IV that the most detrimental impact of advanced DSM is found in Case 1 when the system is free of RES-based generation. When the system RES baseline increases to 30% (Case 2), the overall impact of advanced DSM becomes positive (beneficial); however, advanced DSM deteriorates combined system stability again when the RES baseline further increases to 60% (Case 3). Furthermore, the detrimental impact of advanced DSM in case of high RES penetration levels is further enlarged by increased DSM capacity (Case 5) and changed DSM location (Case 4). It should be noted here that in Cases 1 to 3 and Cases 5 to 6, the total amount available for DSM deployment across the network is 3126 MW (18% of network peak demand). This decreases to 820 MW (5% of network peak demand) in Case 4 due to the changes of DSM deployment locations and nominal power of DSM assets. Therefore, DSM deployed at locations in Case 4 is more effective than at locations in other cases in terms of changing combined system stability performance.

TABLE IV: QUANTIFIED OVERALL IMPACT OF ADVANCED DSM ON COMBINED SYSTEM STABILITY FOR ALL CASE STUDIES

Case Studies	Quantified Impact of Advanced DSM
Case 1	-0.54
Case 2	+0.32
Case 3	-0.24
Case 4	-0.37
Case 5	-0.28
Case 6	+1.03
Case 7	-0.02

Regarding Case 6, advanced DSM significantly improves combined system stability performance throughout the day. The beneficial impact of advanced DSM in the case of composite load model is more significant than all other detrimental impacts observed from other study cases. The significant qualitative difference in the impact of advanced DSM in Cases 3 and 6 emphasises the importance of accurate modelling of demand when studying the impact of DSM on system stability performance. Finally, the impact of advanced DSM in the 4TNE system (Case 7) is found to be minor due to the limited DSM implementation (14 out of 24 hours rather than 23 out of 24 hours in the case of the IEEE 68-bus test system) dictated by the smaller size, availability and flexibility of the real-world DSM assets, relatively smaller size of actual system disturbances and much lower penetration of RES that impacts the overall system dynamic response.

VI. Discussion

The proposed composite stability index (PCICSI) balances different and sometimes opposite impacts of advanced DSM on different stability aspects and clearly indicates the potential risk of violating system stability limit. Thus, it provides an efficient way for system operators to implement and plan corresponding DSM programs by considering contributions to overall system performance. The overall impact of DSM programs can be estimated and studied based on the variation of PCICSI, such that system operators can clearly understand the impact of deployed or upcoming DSM programs. The index can be further tailored to particular system characteristics by introducing appropriate weighting factors (based on experience or following implementation of advanced machine learning methodologies to learn from past system performance) for different stability aspects considered. At present, the best stability performance with respect to different types of stability, which can be considered as extreme events, has been adopted as the reference value. As such, the application of PCICSI does not rely on huge historical data. The computational cost of updating reference values, if needed, is relatively low because the best stability performances are only required to be updated when new extreme events appear.

Because all individual stability indices and corresponding stability limits can be easily changed without any loss of generality, the proposed PCICSI framework can be extended to any power system and adopted in other types of power system analyses as well as in studies beyond power systems.

However, PCICSI is more suitable for assessing the impact of DSM at planning stage, rather than monitoring real-time system stability performance, due to the lack of appropriate reference values. Additionally, this paper considered that all individual stability indices are equally weighted and independent, to illustrate the feasibility of application of the PCICSI. Developing appropriate weighting factors for individual stability indices for more accurate assessment of DSM contribution to system stability, and other system performance attributes, would be necessary for application in specific power systems and could be informed by particular system characteristics based either on the operator's experience or following implementation of advanced machine learning methodologies to learn from past system performance data. This would increase the accuracy and suitability of PCICSI application in real systems.

Moreover, the comprehensive modelling of DSM introduced in this paper can also be used in other areas of power system operation (e.g., congestion management, voltage regulation, assessment of losses and economic analysis of DSM deployment) beyond system angular and frequency stability illustrated in this paper.

The assessment of the impact of advanced DSM on combined system stability for application in practical systems can be further improved by including voltage stability and by assessing the sensitivity of the impact of DSM to modelling parameters of DSM programs (e.g., maximum shiftable time). These aspects, however, were beyond the scope of the study presented in this paper.

In addition to the relatively minor technical limitations for immediate application of the proposed framework in the practical systems, the key limitation is the lack of an appropriate regulatory framework. The main barrier for application of advanced, or any other, DSM programs, in particular, but not limited to those related to harnessing services from customers connected to distribution network, is the establishment of appropriate regulatory framework for provision of ancillary services. This would regulate the cash flow between the provider and user of the service and stimulate participation in any further development of DSM programs. The technical barriers associated with this regulatory barrier include the establishment of appropriate communication networks between the system operator and providers of the service and suitable software platform that would facilitate the observability and controllability of available flexible assets by the system operator, or aggregator if the provision of the services is sub-contracted to the aggregator.

Conclusion

This paper investigates the overall impact of advanced DSM on combined system stability assessed by a composite stability index (i.e., PCICSI) under various operating conditions with the consideration of critical operating uncertainties.

The proposed composite stability index assesses multiple stability aspects simultaneously relying on normalised stability distances calculated based on widely adopted individual stability indices from corresponding stability aspects. The PCICSI has been proven to be efficient to combine and balance different and even opposite impacts of advanced DSM on individual stability aspects, to clearly illustrate the variations of combined system stability performance and to identify unstable operating conditions based on a widely adopted IEEE test system and an equivalent representation of real interconnected systems. The proposed framework relying on PCICSI and comprehensive modelling of DSM can be used in other power system analyses beyond the system stability

with appropriate settings of weights (based on particular system performance criteria and limitations) attached to simultaneously considered system performance attributes.

By investigating and quantifying the overall impact of advanced DSM based on operating conditions with different RES baselines, DSM deployment locations, DSM capacities and load models, it has been found that the system RES baseline and modelling of demand are critical for assessing the DSM impact as variations of these factors can result in qualitative changes (beneficial and detrimental) of the result. DSM locations and DSM capacity mostly affect the magnitude of the impact while the direction of the impact (positive or negative) remains the same. The impact of advanced DSM on stability of the network with low penetration of RES, small capacity of flexible DSM assets and limited DSM implementation is modest. The critical factors affecting the impact of advanced DSM on system stability can help system operators to model, plan and implement DSM programs more efficiently and ensure that system stability is not endangered following the deployment of DSM programs.

REFERENCE

[1] T. Logenthiran, D. Srinivasan and T. Z. Shun, "Demand Side Management in Smart Grid Using Heuristic Optimization," *IEEE Trans. Smart Grid*, vol. 3, no. 3, pp. 1244-1252, June 2012.

[2] C.M. Affonso, L.C.P. da Silva, F.G.M. Lima and S. Soares, "MW and MVar management on supply and demand side for meeting voltage stability margin criteria," *IEEE Trans. Power Systems*, vol. 19, no. 3, pp. 1538-1545, August 2004.

[3] Y. Dong, X. Xie, W. Shi, B. Zhou and Q. Jiang, "Demand-Response-Based Distributed Preventive Control to Imporve Short-Term Voltage Stability," *IEEE Trans. Smart Grid*, vol. 9, no. 5, pp. 4785-4795, February 2017.

[4] J. Hu, J. Cao, J. M. Guerrero, T. Yong and J. Yu, "Improving Frequency Stability Based on Distributed Control of Multiple Load Aggregators," *IEEE Trans. Smart Grid*, vol. 8, no. 4, pp. 1553-1567, November 2015.

[5] M. R. V. Moghadam, R. T. B. Ma and R. Zhang, "Distributed Frequency Control in Smart Girds via Randomized Demand Response," *IEEE Trans. Smart Grid*, vol. 5, no. 6, pp. 2798-2809, May 2014.

[6] X. Tang, J. V. Milanovic, "Assessment of the impact of demand side management on power system small signal stability," *IEEE PowerTech*, Manchester, United Kingdom, June 18-22, 2017.

[7] W. Hu, C. Wang, Z. Chen and B. Bak-Jensen, "Power system transient stability improvement using demand side management in competitive electricity markets," *International Conference on the European Energy Market*, Florence, Italy, May 10-12, 2012.

[8] C. Duan, P. Chakraborty, T. Nishikawa, A. E. Motter, "Hierarchical Power Flow Control in Smart Grids: Enhancing Rotor Angle and Frequency Stability with Demand-Side Flexibility," *IEEE Trans. Control of Network Systems*, vol. 8, no. 3, pp. 1046-1058, April 2021.

[9] S. Ranjan, A. Latif, D. C. Das, N. Sinha, S.M. S. Hussain, T. S. Ustun and A. Iqbal, "Simulataneous analysis of frequency and voltage control of the interconnected hybrid power system in presence of FACTS devices and demand response scheme," *Energy Reports*, vol. 7, pp. 7445-7459, November 2021.

[10] B. Qi, K. N. Hasan and J. V. Milanovic, "Identification of Critical Parameters Affecting Voltage and Angular Stability Considering Load-Renewable Generation Correlations," *IEEE Trans. Power Systems*, vol. 34, no. 4, pp. 2859-2869, January 2019.

[11] K. N. Hasan, R. Preece and J. V. Milanovic, "The Influence of Load on Risk-Based Small-Disturbance Security Profile of a Power System," *IEEE Trans. Power Systems*, vol. 33, no. 1, pp. 557-566, January 2018.

[12] N. Mithulananthan, C. A. Canizares, J. Reeve and G. J. Rogers, "Comparison of PSS, SVC, and STATCOM controllers for damping power system oscillations," *IEEE Trans. Power Systems*, vol. 18, no. 2, pp. 786-792, May 2003.

[13] T. P. Sari, A. Priyadi, V. Lystianingrum, M. H. Purnomo and E. Muljadi, "Utilization of Supercapacity to Extend the Critical Clearing Time in a Power System," *IEEE Open Journal of Industry Applications*, vol. 1, pp. 248-257, November 2020.

[14] J. Huang, L. Guan, Y. Su, H. Yao, M. Guo and Z. Zhong, "Recurrent Graph Convolutional Network-Based Multi-Task Transient Stability Assessment Framework in Power System," *IEEE Access*, vol. 8, pp. 93283-93296, April 2020.

[15] J. I. Yoo, Y. C. Kang, E. Muljadi, K. H. Kim and J. W. Park, "Frequency Stability Support of a DFIG to Improve the Settling Frequency," *IEEE Access*, vol. 8, pp. 22473-22482, January 2020.

[16] B. S. Abdulraheem and C. K. Gan, "Power System Frequency Stability and Control: Survey," *International Journal of Applied Engineering Research*, vol. 11, no. 8, pp. 5688-5695, 2016.

[17] M. Nedd, J. Browell, K. Bell and C. Booth, "Comtaining a Credible Loss to Within Frequency Stability Limits in a Low-Inertia GB Power System," *IEEE Trans. Industry Applications*, vol. 56, no. 2, pp. 1031-1039, April 2020.

[18] R. Urban, S. Denis and M. Rafael, "Estimating frequency stability margin for flexible under-frequency relay operation," *Electric Power Systems Research*, vol. 194, 2021.

[19] Y. Zhu and J. V. Milanovic, "Efficient identification of critical load model parameters affecting transient stability," *Electric Power Systems Research*, vol. 175, 2019.

[20] P. N. Papadopoulos and J. V. Milanovic, "Probabilistic Framework for Transient Stability Assessment of Power Systems With High Penetration of Renewable Generation," *IEEE Trans. Power Systems*, vol. 32, no. 4, pp. 3078-3088, November 2016.

[21] S. Tao, Y Ruoying, Z. Lingzhi and G. Shan, "Power system probabilistic production simulation containing large-scale wind power and photovoltaic power," in *IEEE PES Asia-Pacific Power Energy Eng. Conf. (APPEEC)*, Hong Kong, China, December 8-11, 2013.

[22] M. Fan, V. Vittal, G. Heydt and R. Ayyanar, "Probabilistic power flow stidies for transmission systems with photovoltaic generation using cumulants," *IEEE Trans. Power Systems*, vol. 27, no. 4, pp. 2251-2261, November 2012.

[23] M. Abdraman, A. Tahir, D. Lissouck, M. Kazet and R. Mouangue, "Wind Resource Assessment in the City of N'djamena in Chad," *International Journal of Renewable Energy Research-IJRER*, vol. 6, no. 3, 2016.

[24] R. Preece and J. V. Milanovic, "Tuning of a damping controller for multiterminal VSC-HVDC grids using the probabilistic collocation method," *IEEE Trans. Power Del.*, vol. 29, no. 1, pp. 318-326, Feburary 2014.

[25] M. Starke, N. Alkadi and O. Ma. "Assessment of Industrial Load for Demand Response across U.S. Regions of the Western Interconnect," *ORNL.*, Oak Ridge, Tennessee, USA. September 2013.

[26] The University of Edinburgh, "Matching Renewable Electricity Generation with Demand," *Scottish Executive*, Edinburgh, 2006.

[27] "Monthly Hourly Load Values," entsoe.eu, 2019. [Online]. Available: https://www.entsoe.eu/data/power-stats/hourly load/ [Accessed: 14/10/2019] .

[28] T. Guo and J. V. Milanovic, "Probabilistic framework for assessing the accuracy of data mining tool for online prediction of transient stability," *IEEE Trans. Power Systems*, vol. 29, no. 1, pp. 377-385, January 2014.

[29] T. Muller and D. Most, "Demand Response Potential: Available when Needed? ," *Energy Policy*, vol. 115, pp. 181-198, April 2018.

[30] H. C. Gils, "Assessment of the theoretical demand response potential in Europe," *Energy*, vol. 67, pp. 1-18, April 2014.

[31] H. C. Gils, "Assessment of the theoretical demand response potential in Europe," *ELSEVIER*, Energy 67, pp. 1-18, 2014.

[32] B. Drysdale, J. Wu and N. Jenkins, "Flexible demand in the GB domestic electricity sector in 2030," *ELSEVIER*, Applied Energy 139, pp. 281-290, 2015.

[33] P. Bertoldi, B. Hirl and N. Labanca, "Energy efficiency status report 2012," *European Commission, JRC, Scientific and Policy Reports* 136, 2012.

[34] CIGRE WG C4.605: "Modelling and aggregation of loads in flexible power networks," Jovica V. Milanovic, (Convenor), (TB 566), ISBN: 978-2-85873-261-6, February 2014.

[35] R. Preece and J. V. Milanovic, "Efficient estimation of the probability of small-disturbance instability of large uncertain power systems," *IEEE Trans. Power Systems*, vol. 31, no. 2, pp. 1063-1072, March 2016.

[36] R. D. Zimmerman, C. E. Murillo-sanchez and R. J. Thomas, "MATPOWER: Steady-State Operations, Planning, and Analysis Tools for Power Systems Research and Education," *IEEE Trans. Power Systems*, vol. 26, no. 1, pp. 12-19, June 2010.